Journal of Magnetic Resonance 253 (2015) 154–165

Contents lists available at ScienceDirect

Journal of Magnetic Resonance

journal homepage: www.elsevier.com/locate/jmr

REDOR solid-state NMR as a probe of the membrane locations of membrane-associated peptides and proteins

Lihui Jia, Shuang Liang, Kelly Sackett, Li Xie, Ujjayini Ghosh, David P. Weliky *

Department of Chemistry, Michigan State University, 578 S. Shaw Lane, East Lansing, MI 48824, United States

ARTICLE INFO

Article history:
Received 28 October 2014
Revised 21 December 2014

Keywords:
REDOR
^{13}C
^{2}H
^{31}P
Membrane location
Fusion peptide
Solid-state NMR
NMR

ABSTRACT

Rotational-echo double-resonance (REDOR) solid-state NMR is applied to probe the membrane locations of specific residues of membrane proteins. Couplings are measured between protein ^{13}CO nuclei and membrane lipid or cholesterol ^{2}H and ^{31}P nuclei. Specific ^{13}CO labeling is used to enable unambiguous assignment and ^{2}H labeling covers a small region of the lipid or cholesterol molecule. The ^{13}CO–^{31}P and ^{13}CO–^{2}H REDOR respectively probe proximity to the membrane headgroup region and proximity to specific insertion depths within the membrane hydrocarbon core. One strength of the REDOR approach is use of chemically-native proteins and membrane components. The conventional REDOR pulse sequence with 100 kHz ^{2}H π pulses is robust with respect to the ^{2}H quadrupolar anisotropy. The ^{2}H T_1's are comparable to the longer dephasing times (τ's) and this leads to exponential rather than sigmoidal REDOR buildups. The ^{13}CO–^{2}H buildups are well-fitted to $A \times (1 - e^{-\gamma\tau})$ where A and γ are fitting parameters that are correlated as the fraction of molecules (A) with effective ^{13}CO–^{2}H coupling $d = 3\gamma/2$. The REDOR approach is applied to probe the membrane locations of the "fusion peptide" regions of the HIV gp41 and influenza virus hemagglutinin proteins which both catalyze joining of the viral and host cell membranes during initial infection of the cell. The HIV fusion peptide forms an intermolecular antiparallel β sheet and the REDOR data support major deeply-inserted and minor shallowly-inserted molecular populations. A significant fraction of the influenza fusion peptide molecules form a tight hairpin with antiparallel *N*- and *C*-α helices and the REDOR data support a single peptide population with a deeply-inserted *N*-helix. The shared feature of deep insertion of the β and α fusion peptide structures may be relevant for fusion catalysis via the resultant local perturbation of the membrane bilayer. Future applications of the REDOR approach may include samples that contain cell membrane extracts and use of lower temperatures and dynamic nuclear polarization to reduce data acquisition times.

The membrane of a cell provides a physical barrier to molecular diffusion because of the stable lamellar bilayer structure formed by lipid and cholesterol (Chol). The membrane also contains many different proteins and the total membrane mass is about equally divided between protein and (lipid + Chol). The locations of specific protein residues relative to specific regions of membrane lipids and cholesterol provide insight into protein/membrane biophysical interaction and for some proteins is important for their function [1–3]. High-resolution protein structures are most commonly generated in non-lamellar media like detergent micelles, detergent-rich bicelles, or lipidic cubic phase. These structures sometimes provide information about the protein location in the non-lamellar phase but typically not in the bilayer phase which is the most relevant model of the cell membrane.

The present perspective describes how residue-specific location in the bilayer phase may be probed with rotational-echo double-resonance (REDOR) measurements of proximities between protein

Abbreviations: δ, chemical shift; γ, buildup rate; τ, REDOR dephasing time; A, buildup extent; Chol, cholesterol; Chol_d6, cholesterol-2,2,3,4,4,6-d6; Chol_d7, cholesterol-25,26,26,26,27,27,27-d7; CP, cross-polarization; d, dipolar coupling; Fmoc, 9-fluorenylmethoxycarbonyl; FP-HP, fusion peptide-hairpin protein; HEPES, 2-[4-(2-hydroxyethyl)piperazine-1-yl]ethanesulfonic acid; HIV, human immunodeficiency virus; HFP, HIV fusion peptide; IFP, influenza virus fusion peptide; *lab*, labeled; MAS, magic angle spinning; MD, molecular dynamics; MES, 2-(*N*-morpholino) ethanesulfonic acid; *na*, natural abundance; *P*, population; PC, phosphatidylcholine headgroup lipid; PC_d4, 1,2-(dipalmitoyl-2,2,2,2-d4)-*sn*-glycero-3-phosphocholine; PC_d8, 1,2-(dipalmitoyl-7, 7,7,7,8,8,8,8-d8)-*sn*-glycero-3-phosphocholine; PC_d10, 1,2-(dipalmitoyl-15,15,15,15,16,16,16,16,16,16,16-d10)-*sn*-glycero-3-phosphacholine; PG, phosphatidylglycerol headgroup lipid; r, internuclear distance; REDOR, rotational-echo double-resonance; RP-HPLC, reversed-phase high-performance liquid chromatography; SSNMR, solid-state nuclear magnetic resonance; tBoc, *t*-butoxycarbonyl.

* Corresponding author. Fax: +1 517 353 1793.
E-mail address: weliky@chemistry.msu.edu (D.P. Weliky).

http://dx.doi.org/10.1016/j.jmr.2014.12.020
1090-7807/

^{13}C and membrane ^{2}H or ^{31}P nuclei [4–6]. This work is done in the context of a variety of other established approaches to probe residue-specific membrane location. For example, the distance between a Trp indole group and a non-native lipid Br atom can be semi-quantitatively determined from Br-induced quenching of the indole fluorescence [2,7,8]. The data are most unambiguously interpreted with a single Trp residue in the protein sequence. This is typically achieved by mutagenesis with a concomitant need to test function of the mutagenized protein. A related EPR-based approach is paramagnetic enhancement of electron-spin T_2 relaxation of the stable organic free radical of a derivatized Cys residue [9,10]. The location of the free radical is derived from comparison between a sample in which the paramagnetic substance is localized to the aqueous environment, e.g. $Ni(EDTA)_3$, and one in which the substance is localized to the membrane hydrocarbon core, e.g. O_2. As with the fluorescence approach, the EPR data are most unambiguously interpreted using protein with a single Cys residue so mutagenesis and functional testing are typically required.

The fluorescence and EPR approaches are high-sensitivity and based on relaxation. Related approaches have been developed for lower-sensitivity SSNMR for which protein with wild-type sequence can be used. The aqueous exposure of a residue is probed by reduction in signal intensity with addition of soluble paramagnetic substances like Mn^{2+} [1,11]. Although the intensity reduction is theoretically ascribed to increased T_2 relaxation and consequent spectral broadening, increased linewidth is not always clearly apparent in the spectrum. A second common approach is measurement of magnetization exchange between ^{1}H's of headgroup water or lipid acyl chains and ^{1}H's of residue sidechains with typical subsequent transfer to ^{13}C nuclei to resolve signals of individual residues [3,12–15]. The ^{13}C signal buildup is fitted with a model of ^{1}H spin diffusion whose rate depends on the closest $^{1}H_{H2O}$–$^{1}H_{protein}$ or $^{1}H_{lipid}$–$^{1}H_{protein}$ distance.

The above-described methods are measurements of relaxation rates, i.e. non-radiative changes in state caused by motion-induced fluctuations of local electric or magnetic fields. The goal is extraction of a specific membrane-residue distance from the relaxation rate via the distance dependence of the local field. The analysis is typically underdetermined because the field also depends on orientation and the rate also depends on the unknown distributions of amplitudes and frequencies of thermally-driven motion. Typically, a single distance or membrane insertion depth is semi-quantitatively extracted even though the rate can sometimes also be described with two or more populations with different distances or depths.

We have pursued protein ^{13}C–membrane ^{2}H or ^{31}P REDOR to probe residue-specific membrane location [5,6,16–18]. We were motivated to use an approach for which there was coherent magnetization transfer between spins and where the data analysis could be validated using protein containing isolated spin pairs with a single dipolar coupling d and internuclear distance r with $d \propto r^{-3}$. The buildup of the experimental $(\Delta S/S_0)^{exp}$ with dephasing time τ is fitted to a long-time extent and buildup rate which are respectively correlated to the fractional population with a particular d. In a membrane protein sample, a ^{13}C is coupled to multiple ^{2}H's or ^{31}P's with different pairwise r's and d's (Fig. 1). The fractional population and effective d and r are semi-quantitatively determined from the extent and buildup rate. The $d \propto r^{-3}$ means that the buildup is typically dominated by the closest ^{2}H or ^{31}P. There is the further possibility of analysis to extract multiple couplings from the buildup [19]. There are several strengths of the REDOR approach including robustness of $(\Delta S/S_0)^{exp}$ with respect to rf fields including ^{1}H decoupling, rf inhomogeneity, resonance offsets, quadrupolar and chemical shift anisotropies, and magic angle spinning (MAS) frequency [20]. Non-chemically modified lipids and Chol are available with a wide variety of ^{2}H labeling patterns located in different bilayer regions (Fig. 1).

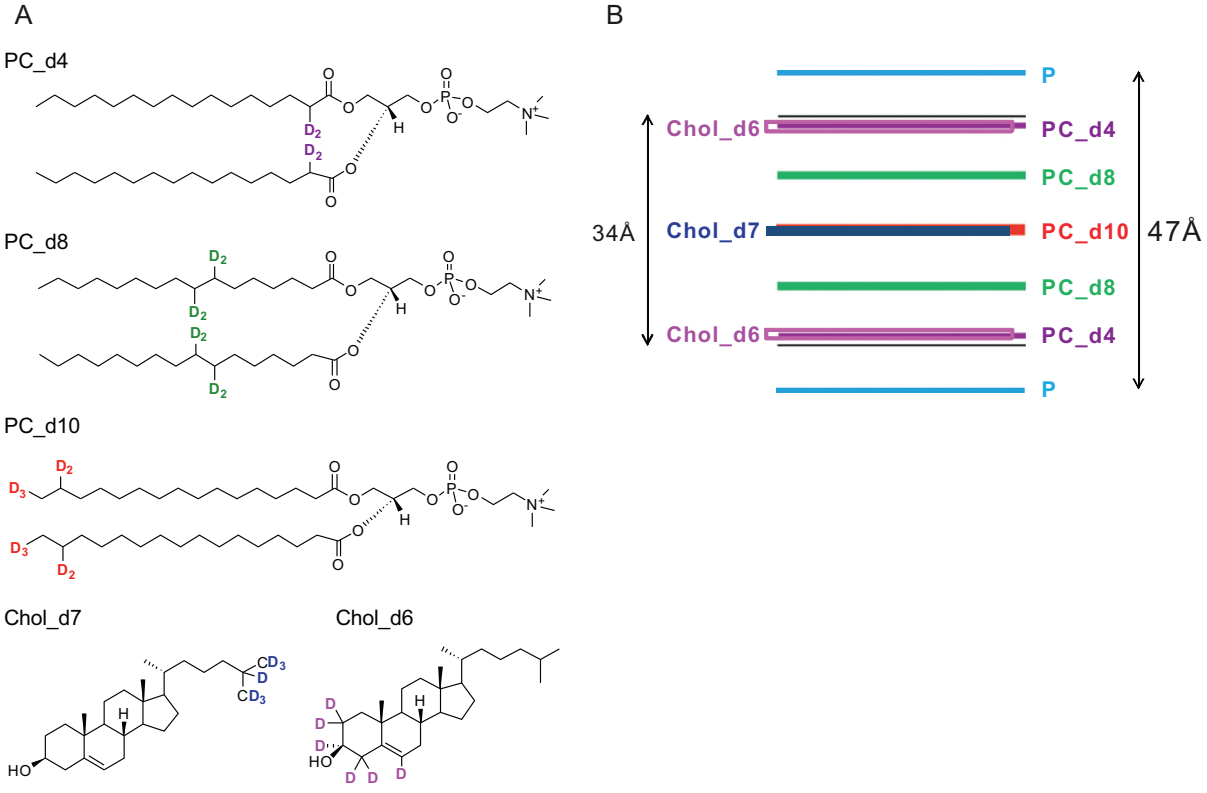

Fig. 1. (A) ^{2}H patterns of lipids and cholesterol and (B) approximate membrane locations of the ^{2}H's and ^{31}P's (P) in the membrane bilayer without protein. The lipid ^{2}H and ^{31}P locations are for the membrane gel-phase without cholesterol and the cholesterol ^{2}H locations are for the liquid-ordered phase with cholesterol [56]. The same color-coding is used in subsequent figures. (For interpretation of the references to color in this figure legend, the reader is referred to the web version of this article.)

Table 1
Protein sequences.

Protein	Sequence[a,b,c]
HFP	AVGIGALFLG FLGAAGSTMG ARS *WKKKKKKG*
HFP_V2E	AEGIGALFLG FLGAAGSTMG ARS *WKKKKKKG*
FP-HP	AVGIGALFLG FLGAAGSTMG ARACTLTVQA RQLLSGIVQQ QNNLLRAIEA QQHLLQLTVW GIKQLQARIL *SGGRGG* WMEWDREINN YTSLIHSLIE ESQNQQEKNE QELLELDKW
IFP	GLFGAIAGFI ENGWEGMIDG *GGKKKKG*

[a] Spaces separate groups of ten native residues.
[b] Underlined residues are ^{13}CO labeled.
[c] Italicized residues are non-native.

The REDOR approach of the present study is applied to domains of the HIV gp41 and influenza virus hemagglutinin proteins that catalyze joining (fusion) of the viral and host cell membranes which is an initial step in infection [21]. The data are obtained for samples containing the ~20-residue *N*-terminal "fusion peptide" domain that binds to the cell membrane and plays an important role in fusion [22,23]. The membrane location(s) of the fusion peptide have been proposed to be a key factor in fusion catalysis because they result in local bilayer perturbation which resembles the fusion transition state with consequent reduction in fusion activation energy [9,10,24–27]. There are different sequences for the HIV (HFP) and influenza (IFP) fusion peptides as well as the fusion-impaired HFP_V2E point mutant (Table 1) [28]. The HFP and IFP samples are respectively prepared at pH 7 and 5 which reflects the expected pH's for viral fusion with the plasma and late endosomal membranes. Membrane-associated HFP typically forms a small intermolecular antiparallel β sheet with a distribution of antiparallel registries [29,30]. IFP forms both this β structure as well as a monomeric hairpin structure containing closely-packed antiparallel *N*- and *C*-helices [27,31–33]. The ^{13}CO–^{31}P REDOR experiments were done with a much larger "FP-HP" region of gp41 that includes the HFP (Table 1) [34]. The FP-HP samples were prepared at pH 3 rather than pH 7 to create positively-charged protein with consequent higher binding to the negatively-charged membrane and reduced protein aggregation in aqueous solution [35–37]. Similar ^{13}CO–^{31}P REDOR data have been obtained for the HFP region of FP-HP at pH's 3 and 7 [35].

1. Experimental

1.1. Materials

Most Fmoc and tBoc amino acids and resins were obtained from Novabiochem, Peptides International, Sigma–Aldrich and Dupont. 1-^{13}C labeled amino acids were obtained from Cambridge Isotopes or Sigma–Aldrich. The tBoc protection of labeled amino acids was done in our laboratory. Lipids were obtained from Avanti Polar Lipids. The phosphatidylcholine headgroup lipid (PC) was typically 1,2-dipalmitoyl-*sn*-glycero-3-phosphocholine and the phosphatidylglycerol headgroup lipid (PG) was typically 1,2-dipalmitoyl-*sn*-glycero-3-phospho-(1′-*rac*-glycerol) (sodium salt). PC_d4, PC_d8, and PC_d10 were custom-synthesized by Avanti using deuterated palmitic acids obtained from CDN isotopes (Fig. 1). Other reagents including cholesterols with ^{2}H labeling were typically obtained from Sigma–Aldrich.

1.2. Peptide and protein synthesis

HFP, HFP_V2E, and IFP were synthesized manually with solid-phase peptide synthesis (Table 1) [38]. Peptide purification was done with reversed-phase HPLC with final purity of >95% verified by mass spectrometry. Hairpin (HP) protein was synthesized recombinantly in bacteria and purified by RP-HPLC. FP-HP protein was synthesized by native chemical ligation of HFP and HP and purified by RP-HPLC [34]. Peptide and protein were quantitated by A_{280} absorbance.

1.3. SSNMR sample preparation

Most HFP samples were made by organic cosolubilization of lipid and HFP to achieve thermodynamic equilibrium integration of the two components. Lipid (~50 μmole) was first dissolved in chloroform and solvent was removed under a stream of nitrogen followed by overnight vacuum pumping. HFP (~1.5 μmole) and lipid film were then dissolved in a solvent mixture containing 2,2,2-trifluoroethanol, 1,1,1,3,3,3-hexafluoroisopropanol, and chloroform with 2:2:3 volume ratio with subsequent solvent removal. The dried film was suspended in ~3 mL aqueous buffer containing 5 mM HEPES and 10 mM MES at pH 7.4 with 0.01 % NaN_3 preservative. After ten freeze/thaw cycles, ~20 mL more buffer was added followed by ultracentrifugation at ~270,000*g* for four hours at 4 °C to pellet membrane with bound HFP. Unbound HFP remained in the supernatant and was quantitated using A_{280} and ε_{HFP} = 5900 M^{-1} cm^{-1}. The quantity of membrane-bound HFP was considered to be the difference between the total and unbound quantities and a typical sample contained ~1 μmole bound HFP.

Achievement of the thermodynamic equilibrium location of HFP in the membrane was examined by comparison with a very different incorporation approach which is more like incorporation during viral fusion. The lipid was dissolved in chloroform followed by removal of solvent. Dried lipid was suspended in ~2 mL aqueous buffer and homogenized with freeze/thaw cycles. Unilamellar vesicles were made by repeated extrusion of the lipid suspension through a polycarbonate filter with 100 nm diameter pores. HFP was incorporated into the vesicles by dropwise addition of ~100 μM stock HFP solution into the vesicle suspension while maintaining the pH at 7.4. The mixture was gently vortexed overnight and then treated like the suspension formed after organic cosolubilization.

IFP samples were made by aqueous binding to vesicles at pH 5.0 which is close to the pH of influenza viral fusion in late endosomes. FP-HP samples were also made with this approach and all solutions were buffered with 10 mM formate at pH 3.0. Low pH is needed for protein solubility and also aids binding via electrostatic attraction between positively-charged protein and negatively-charged vesicles [37]. FP-HP, HFP, and IFP typically induce significant fusion of vesicles in aqueous solution, and such fusion is visually observable as increased turbidity of the solution.

1.4. SSNMR spectroscopy

Experiments were done with a 9.4 T Agilent Infinity Plus spectrometer using a ^{1}H/^{13}C/^{2}H or a ^{1}H/^{13}C/^{31}P triple-resonance MAS probe. The sample was typically cooled with nitrogen gas at −50 °C with corresponding sample temperature of ~−30 °C. The REDOR pulse sequence was in time: (1) ^{1}H π/2 pulse; (2) ^{1}H–^{13}C cross polarization (CP); (3) dephasing period of duration τ; and (4) ^{13}C detection (Fig. 2). S_0 and S_1 REDOR data were acquired alternately and differed in the pulses applied during the dephasing period. For both acquisitions, there was a ^{13}C π pulse at the end of each rotor cycle except the last one and for S_1, there was also a ^{2}H or ^{31}P π pulse at the midpoint of each cycle. Typical parameters included: (1) 8–10 kHz MAS frequency and 1.5 ms CP contact time; (2) 50 kHz ^{1}H π/2 pulse and CP; (3) 55–66 kHz ^{13}C CP ramp; (4) 60 kHz ^{13}C π pulses, 100 kHz ^{2}H π pulses, and 63 kHz ^{31}P π pulses with XY-8 phase cycling applied to all π pulses; and ~70 kHz two-pulse phase-modulated ^{1}H decoupling during dephasing and acquisition [39,40]. Typical recycle delays were 1 s (τ = 2, 8,

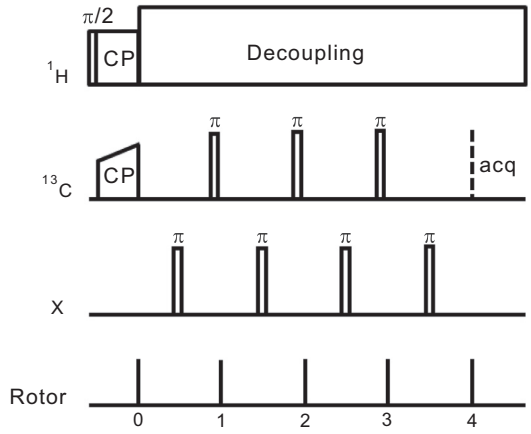

Fig. 2. REDOR S_1 pulse sequence with X ≡ ^{2}H or ^{31}P, CP ≡ cross-polarization, and acq ≡ acquisition.

16 ms), 1.5 s (τ = 24, 32 ms), and 2 s (τ = 40 and 48 ms). The typical numbers of summed S_0 or S_1 scans were ~4000, 7000, 12,000, 25,000, 32,000, 40,000 and 50,000 for τ = 2, 8, 16, 24, 32, 40 and 48 ms, respectively. Data processing included 20–200 Hz Gaussian line broadening and baseline correction. Chemical shift referencing was done externally using adamantane. The methylene ^{13}C shift was set to 40.5 ppm so that shifts can be directly compared to liquid-state NMR shift databases [41].

1.5. Data analysis

The S_0 and S_1 peak intensities are also denoted S_0 and S_1 and are obtained from 1 to 3 ppm integration windows of the isotropic ^{13}CO peaks. The buildup of experimental dephasing $(\Delta S/S_0)^{exp} = (S_0 - S_1)/S_0$ vs τ of a sample provides the basis for assessing the protein labeled (*lab*) ^{13}CO-to-lipid ^{2}H or ^{31}P proximity and r values. The $(\Delta S/S_0)^{exp}$ uncertainty is based on spectral noise [42]. The data are fitted with three approaches that are denoted ***I***, ***II***, and ***III*** and best-fit parameters correspond to the minimum χ^2 value. For ***I*** and ***II***, two- and three-populations of peptides are respectively considered. For each population, the $(\Delta S/S_0)$ are quantum mechanically calculated with the SIMPSON program using a model of isolated spin-pairs with a single value of d [43]. For ***III***, the $(\Delta S/S_0)^{exp}$ are fitted to a single exponential buildup $A \times (1 - e^{-\gamma\tau})$ with A and γ as fitting parameters (Table 2). A is assigned as the approximate fraction of protein with $d \approx 3\gamma/2$ which is based on equal time spent in the three ^{2}H m states during τ because of T_1 relaxation. $(1 - A)$ is the fraction protein with $d \approx 0$.

2. Results

2.1. Features of ^{13}CO–^{2}H REDOR spectra, buildups, and fittings

Fig. 3 presents a representative ^{13}CO–^{2}H $(\Delta S/S_0)^{exp}$ buildup and three fittings as well as the τ = 40 ms REDOR spectra. The sample contains HFP_G5$_C$ and PC_d10 lipid and the S_0 spectrum has a prominent spectral feature with δ_{peak} = 171 ppm that corresponds to *lab* G5 nuclei with β sheet conformation [44]. One advantage of *lab* Gly is that its β sheet ^{13}CO signal is well-resolved from natural abundance (*na*) ^{13}CO signals of other amino acid types and lipid. The S_0 spectrum has a small downfield shoulder that corresponds to *na* HFP and lipid signal. Spin counting supports a ~1:1 *na*:*lab* peak ratio which is very different than the ~1:4 experimental ratio. For smaller τ, larger ratios are observed, consistent with $T_{2,lipid} < T_{2,HFP}$. A similar change in ratio with τ is observed for the monomeric α helical KALP peptide in membranes [6].

Table 2
Best-fit exponential buildup parameters for ^{13}CO–^{2}H REDOR.[a,b]

Peptide	Peak[c]	Membrane	A	γ (Hz)	r (Å)
HFP_G5$_C$	*lab* β	PC_d8	0.60(3)	34(3)	4.5(1)
HFP_G5$_C$	*lab* β	PC_d10	0.63(4)	44(5)	4.1(2)
HFP_G5$_C$	*lab* β	PC_d8:PG (4:1)	0.44(6)	27(6)	4.9(3)
HFP_G5$_C$	*lab* β	PC_d10:PG (4:1)	0.89(2)	36(2)	4.4(1)
HFP_L12$_C$	*lab* β	PC_d8:PG (4:1)	0.50(8)	25(5)	5.0(4)
HFP_L12$_C$	*lab* β	PC_d10:PG (4:1)	0.88(5)	31(3)	4.6(2)
HFP_V2E_G5$_C$	*lab* β	PC_d8:PG (4:1)	0.70(3)	35(3)	4.5(1)
HFP_V2E_G5$_C$	*lab* β	PC_d10:PG (4:1)	0.82(4)	51(4)	4.0(1)
HFP_G5$_C$	*lab* β	PC:PG:Chol_d7 (8:2:5)	0.76(3)	47(3)	4.0(1)
HFP_G16$_C$	*lab* β	PC:PG:Chol_d6 (8:2:5)	0.67(5)	64(10)	3.6(2)
IFP_L2$_C$[d]	*lab* α	PC_d10:PG (4:1)	1.00(15)	38(10)	4.4(4)
IFP_A7$_C$[d]	*lab* α	PC_d10:PG (4:1)	0.99(10)	30(5)	4.7(3)
IFP_A7$_C$[d]	*lab* β	PC_d8:PG (4:1)	0.47(6)	25(5)	5.0(4)
IFP_A7$_C$[d]	*lab* β	PC_d10:PG (4:1)	0.90(19)	23(7)	5.1(5)
HFP_G5$_C$[d]	*lab* β	PC_d10:PG (4:1)	0.70(2)	68(4)	3.6(1)
HFP_G5$_C$[e]	*lab* β	PC_d10:PG (4:1)	0.74(10)	30(6)	4.7(3)

[a] Unless otherwise noted, samples were prepared by organic co-solubilization and spectra were obtained at ~−30 °C sample temperature.
[b] The $(\Delta S/S_0)^{exp}$ buildup was fitted to $A \times (1 - e^{-\gamma\tau})$ and r was calculated as $[4642\ \text{Hz}/(3\gamma/2)]^{1/3}$ which is the expression for a single ^{13}CO–^{2}H spin pair. The fittings were statistically reasonable as evidenced by best-fit χ^2 typically between 2 and 10 and therefore close to the number of degrees of freedom ≡ 5.
[c] *lab* α ≡ labeled α helical signal and *lab* β ≡ labeled β sheet signal.
[d] These samples were prepared by aqueous binding peptide to membrane vesicles.
[e] These spectra were acquired at ~0 °C sample temperature.

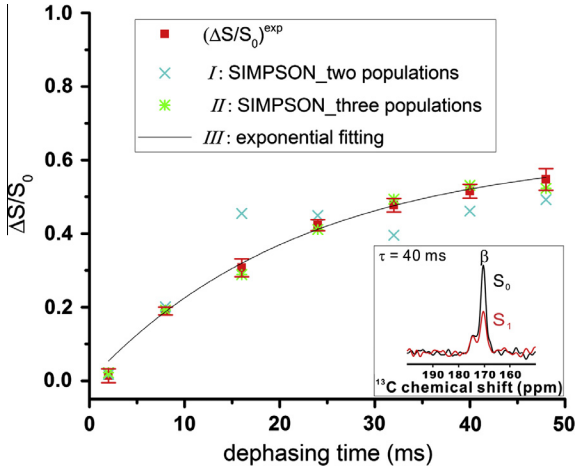

Fig. 3. Experimental ^{13}CO–^{2}H $(\Delta S/S_0)^{exp}$ vs τ (filled red squares with error bars) for a sample that contains HFP_G5$_C$ in PC_d10 membrane. The inset displays the S_0 (black) and S_1 (red) spectra for τ = 40 ms. The $(\Delta S/S_0)^{exp}$ are for the marked *lab* G5 peak corresponding to β sheet structure. Fitted $(\Delta S/S_0)$ are displayed from three different fitting approaches denoted *I*, *II*, and *III*. The blue crosses (*I*) and green stars (*II*) are respectively based on models of two- (P_1 and P_2) and three-populations (P_1, P_2, and P_3) of HFP_G5$_C$ molecules. The $(\Delta S/S_0)$ for each population is calculated with the quantum mechanics-based SIMPSON program using a model of isolated ^{13}CO–^{2}H spin-pairs with a single dipolar coupling (d). For *I*, the best-fit parameter values for P_1 are d = 54 Hz and fractional population A = 0.69. The corresponding P_2 values are set to d = 0 Hz and $1 - A$ = 0.31. For *II*, the best-fit values are d_1 = 90 Hz, A_1 = 0.27, d_2 = 25 Hz, and A_2 = 0.50 with P_3 values set to d_3 = 0 Hz and $A_3 = 1 - A_1 - A_2$ = 0.23. The black line (*III*) is the best-fit to the exponential buildup function $A \times (1 - e^{-\gamma\tau})$ with γ = 44 Hz and A = 0.63. (For interpretation of the references to color in this figure legend, the reader is referred to the web version of this article.)

The buildup of $(\Delta S/S_0)^{exp}$ vs τ of the *lab* G5 β ^{13}CO signal is rapid with an asymptotic value of ~0.6. This value likely reflects the fraction of HFP molecules in contact with at least one D10 ^{2}H because: (1) the asymptotic value varies with *lab* site and with the lipid deuteration pattern (see below); and (2) for a membrane with lipid with perdeuterated acyl chains, the asymptotic value is 1.0 which

indicates that all HFP are inserted into the membrane hydrocarbon core [20]. There was typically <0.02 difference between the $(\Delta S/S_0)^{exp}$ of replicate samples for a given τ.

REDOR buildups have typically been fitted to yield precise distances, e.g. the ^{13}CO-detect/^{15}N-dephase buildup of a *lab* $^{13}CO_{res.\ i}$, $^{15}N_{res.\ i+4}$ α helical peptide is well-fitted with a single $d = 45$ Hz and corresponding $r = 4.1$ Å that support α helical structure in all molecules [42]. The fittings of peptide *lab* ^{13}CO–membrane ^{2}H buildups are different for several reasons. (1) The membrane environment is locally non-crystalline so that the distance between the *lab* ^{13}CO and a particular ^{2}H will vary among peptide molecules even if all the *lab* ^{13}CO's have the same membrane insertion depth. (2) The lipid or Chol contains multiple ^{2}H's and the $(\Delta S/S_0)^{exp}$ of a particular peptide reflects the r's and relative angles of several ^{13}CO–^{2}H internuclear vectors. The multi-spin geometry will also differ among peptide molecules. This effect is mitigated by $d \propto r^{-3}$ for each spin pair so that the $(\Delta S/S_0)^{exp}$ buildup for a molecule is expected to be dominated by the d associated with the closest ^{2}H. This dominance is supported by typical best-fit $r \approx 4$–5 Å that are comparable to the van der Waals separation between *lab* ^{13}CO and lipid ^{2}H's (Table 2). (3) Because the ^{2}H $T_1 \approx 50$ ms, there are $m = 0 \leftrightarrow m = \pm 1$ ^{2}H transitions during the dephasing period [20]. There is not buildup for a *lab* ^{13}CO during the $m = 0$ times. The stochastic variability of the $m = 0$ times among the sample ^{13}CO's is not straightforwardly incorporated into quantum mechanical calculation of the buildup. We approximate that each ^{2}H is in the $m = 0$ state for 1/3 of the dephasing period so that the observed buildup rate $\gamma \approx 2d/3$. This relationship was observed for the buildup of a sample containing isolated ^{13}CO–^{2}H intra-peptide spin pairs with a single r [20]. Overall, these considerations for peptide ^{13}CO–lipid ^{2}H REDOR imply that fitting parameters will be semi-quantitatively rather than quantitatively related to membrane location.

Three fitting approaches denoted ***I***, ***II***, and ***III*** were tried for the HFP_G5$_C$/PC_d10 buildup (Fig. 3). ***I*** considers two populations (P's) of HFP_G5$_C$ molecules. P_1 has *lab* G5 ^{13}CO–lipid ^{2}H proximity that is approximated by isolated spin pairs with a single d whose buildup is calculated quantum–mechanically with the SIMPSON program. The $m = 0 \leftrightarrow m = \pm 1$ non-radiative transitions are not considered in the calculation. P_2 does not have ^{13}CO–^{2}H proximity so $d = 0$ and there is no buildup. The two P_1-associated fitting parameters are d and $A \equiv$ fractional population with $1 - A$ corresponding to the P_2 fractional population. The data are fitted poorly by ***I*** in part because the $(\Delta S/S_0)^{exp}$ buildup has exponential shape whereas the calculated buildup has sigmoidal shape. Better fitting is obtained with ***II*** which considers three populations with four fitting parameters: fractional populations A_1 and A_2; and couplings d_1 and d_2. The $A_3 = 1 - A_1 - A_2$ and $d_3 = 0$. Good fitting is also obtained with ***III***, a single exponential buildup, $A \times (1 - e^{-\gamma\tau})$, with A and γ as fitting parameters. ***III*** is consistent with a model of two populations. P_1 has fraction A and ^{13}CO–^{2}H proximity with $d \approx 3\gamma/2$ and P_2 has fraction $1 - A$ and $d \approx 0$. An r is calculated from the d of P_1 using the approximation of a dominant contribution from coupling to the closest ^{2}H.

We have several reasons for choosing ***III*** rather than ***II*** for general fitting of sample buildups. (1) For most data sets, the χ^2_{III} is lowest and also statistically reasonable because it is close to the number of degrees of fitting $\equiv 5$ [42]. This is achieved with two rather than four fitting parameters and this difference is especially relevant because of only seven data. It is simpler and probably more biophysically plausible to have two rather than three membrane locations. Finally, exponential time dependence is commonly observed for stochastic processes such as the non-radiative $m = 0 \leftrightarrow m = \pm 1$ transitions.

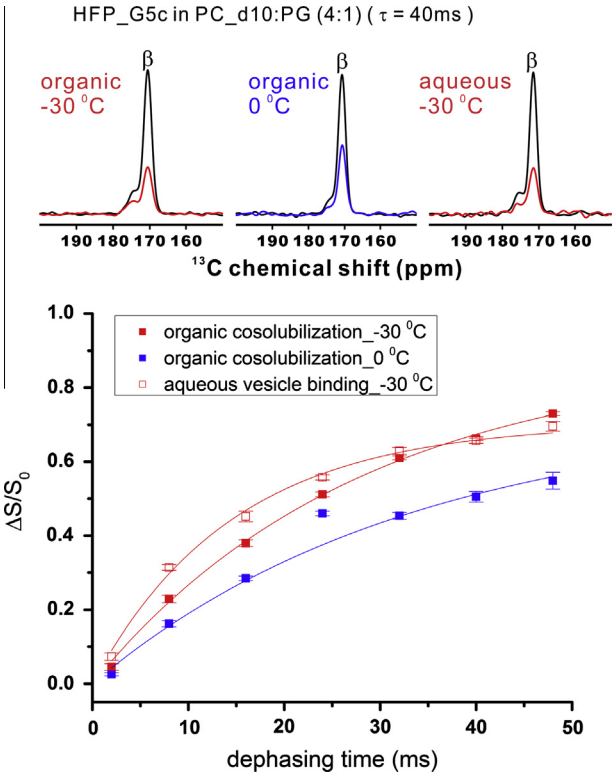

Fig. 4. ^{13}CO–^{2}H REDOR data from samples that contain HFP_G5$_C$ in PC_d10:PG (4:1) membrane. The S_0 (black) and S_1 (colored) REDOR spectra for $\tau = 40$ ms are displayed as well as plots of $(\Delta S/S_0)^{exp}$ vs τ for the *lab* G5 β peak. The solid lines are the best-fit exponential buildups. The displayed experimental uncertainties are comparable to the size of the symbols. The red and blue filled squares are for a sample prepared by organic co-solubilization of HFP and lipid. The red open squares are for a sample prepared by binding HFP to membrane vesicles in aqueous solution. The approximate sample temperatures during REDOR data acquisition were ~−30 °C (red squares) and 0 °C (blue squares). The $\tau = 24$ ms datum is not included in the 0 °C fitting. (For interpretation of the references to color in this figure legend, the reader is referred to the web version of this article.)

2.2. Effects of sample preparation method and temperature

Fig. 4 displays $\tau = 40$ ms REDOR spectra and $(\Delta S/S_0)^{exp}$ buildups for samples at ~−30 °C and containing HFP_G5$_C$ and PC_d10:PG (4:1). One sample was prepared by organic co-solubilization of HFP and lipid and one by binding in aqueous solution. There are comparable buildups for the G5 β feature with very similar $(\Delta S/S_0)^{exp} \approx 0.7$ for large τ. This indicates comparable fractions of molecules with G5 ^{13}CO/PC_d10 ^{2}H contact. The buildup rate is faster for aqueous relative to organic incorporation with respective r of 3.6 and 4.4 Å calculated from the best-fit γ (Table 2). Both r's reflect approximate van der Waals contact between the G5 residue and the PC_d10 ^{2}H nuclei. The similar spectra and buildups for the two different preparation methods support achievement of thermodynamic equilibrium peptide structure and membrane location.

REDOR spectra and buildups are compared for the organic co-solubilization sample cooled with either −50 °C or −20 °C nitrogen gas with corresponding sample temperatures of ~−30 °C and ~0 °C. There is smaller buildup at higher temperature with $[(\Delta S/S_0)^{exp}{}_{0°C}/(\Delta S/S_0)^{exp}{}_{-30°C}] \approx 0.7$ for a given τ. There is also a τ-dependent reduction in S_0 signal-per-scan with increased temperature, e.g. $[(S_0)_{0°C}/(S_0)_{-30°C}]$ is 1.0 for $\tau = 2$ ms and 0.13 for $\tau = 48$ ms. This indicates shorter ^{13}CO T_2 with increased temperature and temperature-independent ^{1}H → ^{13}CO CP. The reduced T_2 is likely a result of increased HFP motion and the reduced REDOR

buildup is probably due to motional averaging of the ^{13}CO–^{2}H dipolar interaction from increased HFP and lipid motions. The other spectra in the present study were acquired with a sample temperature of ~−30 °C.

2.3. Effect of membrane charge

Fig. 5 displays spectra for $\tau = 40$ ms and buildups for HFP_G5$_C$ bound to membranes containing (A) only zwitterionic PC lipid and (B) PC and anionic PG lipids in 4:1 M ratio. Anionic lipid was included because membranes of most human cells including host cells of HIV contain 0.1–0.2 mol fraction anionic lipid [45]. For a given starting quantity of HFP, there is a greater bound fraction for membranes containing anionic lipid likely because of electrostatic attraction between the positively-charged HFP and negatively-charged membrane. Extra HFP was added in preparation of the pure PC samples to compensate for this binding difference. As noted in the Experimental section, the NMR sample was the centrifugation pellet containing membrane + bound peptide. The sample did not contain the unbound HFP which was in the supernatant. The S_0 spectra of both HFP_G5$_C$ samples are similar and have a prominent feature with $\delta_{peak} = 171$ ppm that is assigned to *lab* G5 ^{13}CO's with β sheet structure. There is also similarity between the corresponding buildups with both samples showing substantial buildup in membranes with PC_d8 and PC_d10 lipids and negligible buildup with PC_d4 lipid. These results support insertion of the antiparallel intermolecular HFP β sheet into the membrane hydrocarbon core. Subsequent samples were made with PC:PG (4:1) because of the better protein binding.

2.4. Multiple membrane locations of HFP

Fig. 5B, C shows very similar buildups of HFP_G5$_C$ and HFP_L12$_C$ in PC:PG membranes with greater buildup with PC_d10 than with PC_d8. A similar buildup difference has also been observed for HFP_F8$_C$ [20]. The fittings reveal similar buildup rates for the PC_d8 and PC_d10 samples with $A_{d10}/A_{d8} \approx 2$ (Table 2). This supports two different membrane locations for HFP with a major population with deep insertion in contact with d10 ^{2}H's and a minor population with shallower insertion in contact with d8 ^{2}H's. There is a distribution of lengths of antiparallel HFP registries and the multiple HFP locations may be related to hydrophobicity differences among these registries [30].

2.5. Deep insertion of HFP_V2E_G5$_C$

V2E is the most important engineered mutation of HIV gp41 with impairment of fusion and infection for viruses with a small fraction of V2E mutant and the remainder wild-type gp41 protein [28]. The wild-type and V2E mutant peptides have been proposed to exhibit differences in both backbone conformation and membrane location but in our view, the biophysical basis for the functional impairment by this *N*-terminal mutation is not yet understood [25,46,47]. Fig. 5B, D shows that the S_0 spectra of both peptides have a dominant feature with $\delta_{peak} = 171$ ppm that correlates to a major population with β sheet structure at G5. The downfield feature is stronger for the V2E mutant (most clearly seen for the PC_d4 samples) and correlates to a minor molecular population with α helical G5 structure which is consistent with an earlier study [25]. There are substantial buildups for PC_d8 and PC_d10 samples of both HFP_G5$_C$ and HFP_V2E_G5$_C$ and little buildup for the PC_d4 samples. This supports insertion into the membrane hydrocarbon core for both peptides. The greater buildup of HFP_V2E_G5$_C$ in PC_d8 may reflect location differences within the core.

2.6. Residue contact with specific regions of cholesterol

Cholesterol (Chol) is an important membrane component and represents ~0.25 mol fraction of the membrane of host cells of HIV and ~0.45 mol fraction of the HIV membrane [45]. Fig. 6 displays spectra and buildups for samples containing HFP_G5$_C$ or HFP_G16$_C$ and membrane with lipid and ~0.3 mol fraction "Chol_d7" or "Chol_d6" which respectively refer to Chol deuterated in the methyl or hydroxyl regions (Fig. 1). The ^{2}H's of Chol_d7 and Chol_d6 are respectively near the center and the edge of the membrane. For either HFP_G5$_C$ or HFP_G16$_C$, the most prominent spectral feature has $\delta_{peak} \approx 171$ ppm which corresponds to Gly β sheet structure. HFP_G16$_C$ also has a feature with $\delta_{peak} \approx 174$ ppm which may correspond to HFP molecules with shorter β sheets that do not include G16. Fig. 6 buildups for the 171 ppm feature are strikingly different for the two peptides. For membranes containing Chol_d7, there are large and small buildups for HFP_G5$_C$ and HFP_G16$_C$, respectively, whereas for membrane containing Chol_d6, the trend is opposite with small and large buildups, respectively. The HFP_G5$_C$ buildups support deep insertion of the G5 residue within the membrane hydrocarbon core for a major fraction of HFP molecules. This is consistent with the buildups of HFP_G5$_C$ and HFP_L12$_C$ in membranes containing deuterated lipids (Fig. 5B, C). The HFP_G16$_C$ buildups support a headgroup location for G16.

2.7. Membrane location model for HFP

We propose models for the overall membrane locations of the HFP intermolecular antiparallel β sheet based on the ^{13}CO–^{2}H buildups of the present study as well as earlier data (Fig. 7). The interior of the β sheet is located within the hydrocarbon rather than the headgroup region of the membrane. This reflects lower free energy from the hydrophobic effect for the many apolar amino acid sidechains. By contrast, the ends of the β sheet are located in the headgroup rather than the hydrocarbon region. This is understood in terms of the much higher water content of the headgroup region. There is incomplete inter-residue hydrogen bonding for the end residues and lower free energy results from forming additional hydrogen bonds with water. This is not a consideration for the interior residues for which there is approximately complete inter-residue hydrogen bonding. There is a distribution of antiparallel HFP registries and many have G5 and L12 in the interior and G16 near the end of the β sheet. As noted above, the data are most straightforwardly explained by two membrane locations. The major and minor populations have respective deeper and shallower locations in the hydrocarbon core and contact the PC_d10 and PC_d8 ^{2}H's. The number of HFP's in the β sheet is probably small (~10) which is consistent with gp41 oligomerization including formation of a stable dimer-of-trimers of the gp41 ectodomain [36]. Little is known yet about how lipid and cholesterol molecules are displaced by the β sheet and how those in contact with sheet are oriented relative to those in a bilayer without protein. The displayed insertion into a single leaflet is most consistent with the present data but we cannot rule out a transmembrane location [26].

2.8. ^{13}CO–^{31}P REDOR supports membrane insertion of HFP in gp41

^{13}C–^{2}H REDOR should be straightforwardly applicable to probing the membrane locations of a protein if the ^{13}C resonances are unambiguously assigned. Our approach to-date is synthesis of selectively labeled "FP-HP" protein via ligation of HFP with "HP" where HP comprises most of the rest of ectodomain (Table 1). The HFP is chemically synthesized and selectively ^{13}CO labeled and HP is synthesized recombinantly in bacteria without labeling.

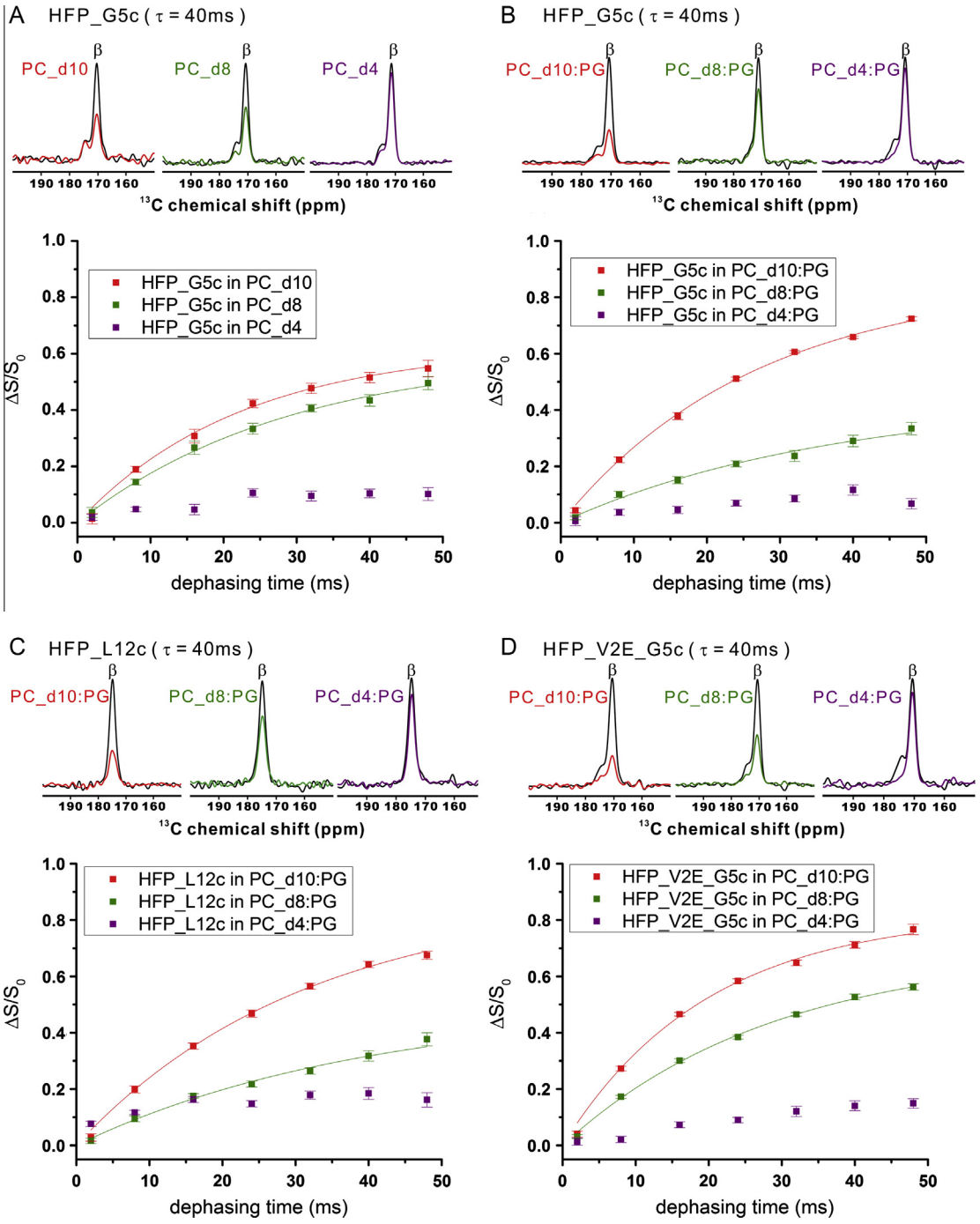

Fig. 5. $^{13}CO–^{2}H$ REDOR data from samples that contain (A) HFP_G5$_C$ in PC, (B) HFP_G5$_C$ in PC:PG (4:1), (C) HFP_L12$_C$ in PC:PG (4:1), and (D) HFP_V2E_G5$_C$ in PC:PG (4:1). Samples were prepared with PC_d4, PC_d8, and PC_d10, and the corresponding data are displayed with colors that match those in Fig. 1. The S_0 (black) and S_1 (colored) REDOR spectra for $\tau = 40$ ms are displayed as well as plots of $(\Delta S/S_0)^{exp}$ vs τ for the *lab* (A, B, D) G5 β and (C) L12 β peaks. The solid lines are best-fits to $A \times (1 - e^{-\gamma\tau})$ and are done for substantial $(\Delta S/S_0)^{exp}$ buildups. (For interpretation of the references to color in this figure legend, the reader is referred to the web version of this article.)

We have not yet examined FP-HP with $^{13}CO–^{2}H$ REDOR but have probed protein proximity to the membrane headgroups with $^{13}CO–^{31}P$ REDOR (Figs. 1 and 8). The S_0 spectra of the FP-HP_G5$_C$ and FP-HP_A1$_C$ samples both have a feature with $\delta_{peak} \approx 178$ ppm that is assigned to *na* ^{13}CO nuclei mostly in the HP domain [48]. The 178 ppm shift is consistent with the thermostable α helical hairpin fold of HP [34,48]. This assignment to *na* nuclei is also supported by REDOR buildups that are independent of *lab* site. The upfield features in the spectra are assigned to *lab* ^{13}CO nuclei in β sheet HFP domains. This assignment is based on $\delta_{peak} \approx 171$ ppm for FP-HP_G5$_C$ and $\delta_{peak} \approx 173$ ppm for FP-HP_A1$_C$ as well as very similar δ_{peak} values of membrane-associated FP-HP_G5$_C$ and β sheet HFP_G5$_C$. Assignment of the upfield peaks to *lab* nuclei is also consistent with the expectation and observation that *lab* REDOR buildups depend on *lab* site.

The negligible G5 β buildup of FP-HP_G5$_C$ supports a G5 ^{13}CO–membrane ^{31}P separation that is >10 Å. This distance is consistent with a location for G5 of FP-HP in the membrane hydrocarbon core that is similar to G5 in HFP (Figs. 5 and 7). The substantial A1 β buildup is well-fitted to $A \times (1 - e^{-\gamma\tau})$ with best-fit $\gamma = 60$ Hz and

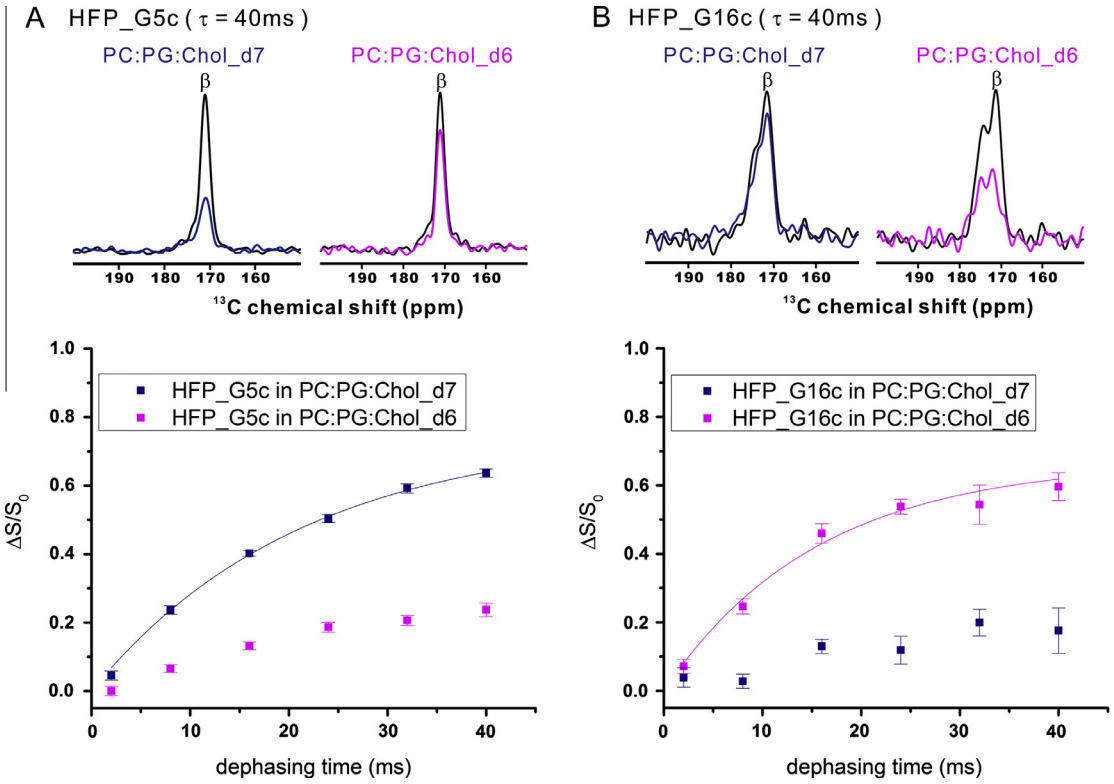

Fig. 6. ^{13}CO–^{2}H REDOR data from samples that contain (A) HFP_G5$_C$ and (B) HFP_G16$_C$ in PC:PG:Chol (8:2:5) membrane. Samples were prepared with Chol_d7 and Chol_d6, and the corresponding data are displayed with colors that match those in Fig. 1. The S_0 (black) and S_1 (colored) REDOR spectra for τ = 40 ms are displayed as well as plots of $(\Delta S/S_0)^{exp}$ vs τ for the *lab* (A) G5 β and (B) G16 β peaks. The solid lines are best-fits to $A \times (1 - e^{-\gamma\tau})$ and are done for substantial $(\Delta S/S_0)^{exp}$ buildups. (For interpretation of the references to color in this figure legend, the reader is referred to the web version of this article.)

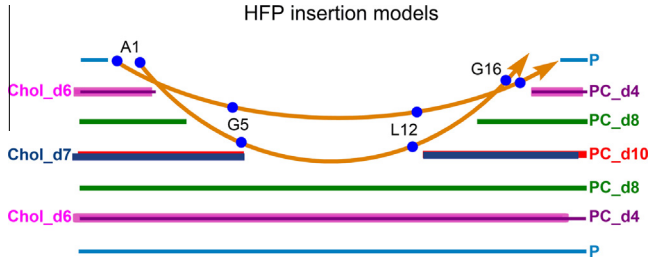

Fig. 7. Semi-quantitative models for deep and shallow HFP membrane insertion that respectively correspond to major and minor HFP populations. Only one HFP molecule is displayed in the small intermolecular antiparallel β sheet. Little is known yet about how lipid and cholesterol molecules are displaced by the β sheet and how those in contact with sheet are oriented relative to those in a bilayer without protein.

A = 0.58. We approximate that $d \approx \gamma$ and calculate $r \approx 5.9$ Å using the r (Å) = (12,250 Hz/d)$^{1/3}$ expression valid for a single ^{13}C–^{31}P spin pair. This analysis supports ~0.6 fraction of FP-HP molecules with van der Waals contact between A1 and the phosphate group and supports an A1 location in the headgroup region. The A1 is at the end of the intermolecular β sheet and a headgroup rather than hydrocarbon location allows hydrogen bonding with water. These FP-HP data suggest that Fig. 7 location model is also representative of β sheet HFP in gp41. This intermolecular antiparallel sheet probably forms during later steps of viral fusion and is likely preceded by folding in the inter-membrane space of the rest of the gp41 ectodomain into a dimer of trimer helical hairpins [35,36]. Such folding likely positions the HFP's in an antiparallel arrangement.

2.9. Membrane insertion of both α helical and β sheet IFP

Fig. 9 displays τ = 40 ms ^{13}CO–^{2}H REDOR spectra and buildups for membrane-associated influenza virus fusion peptides IFP_L2$_C$ and IFP_A7$_C$. There are prominent features in the L2$_C$ and A7$_C$ spectra with respective δ_{peak}'s of ~177 and ~179 ppm that are assigned to a molecular population with α helical structure at L2 and A7 [49]. There are also features with δ_{peak}'s of ~173 and ~174 ppm that are assigned to a separate population with β sheet structure at these residues [44]. Although all samples are prepared with the same protocol, there is some variation in the α:β population ratio. Previous work has shown that the α structure is a monomeric hairpin with *N*-helix (residues 1–11) and *C*-helix (residues 13–19) that are antiparallel and in close contact with one another [27,33]. The overall structure is amphipathic with hydrophobic and hydrophilic sidechains clustered on opposite faces. Much less is known about the β structure but it may be an antiparallel intermolecular β sheet like HFP.

There are large comparable α buildups for IFP_L2$_C$ and IFP_A7$_C$ in membrane containing PC_d10 and much smaller buildups in PC_d8 or PC_d4. These data support one location for the *N*-helix that is near the center of the hydrocarbon core. The best-fit $A \approx 1$ for the PC_d10 samples also supports a single location. Deep rather than interfacial location is supported by comparable L2$_C$ and A7$_C$ buildups even though the L2 and A7 *lab* ^{13}CO nuclei are respectively closer to the hydrophobic and hydrophilic faces of the structure. For membrane that contains PC_d10, there are smaller β than α buildups which supports an overall shallower location for β IFP. The β IFP buildups are typically smaller than the comparable β HFP buildups. However, at least IFP_A7$_C$ shows a buildup pattern similar to those of HFP_G5$_C$ and HFP_L12$_C$ with measurable buildup in membranes containing PC_d10 or PC_d8, and $\gamma_{d10} \approx \gamma_{d8}$ and

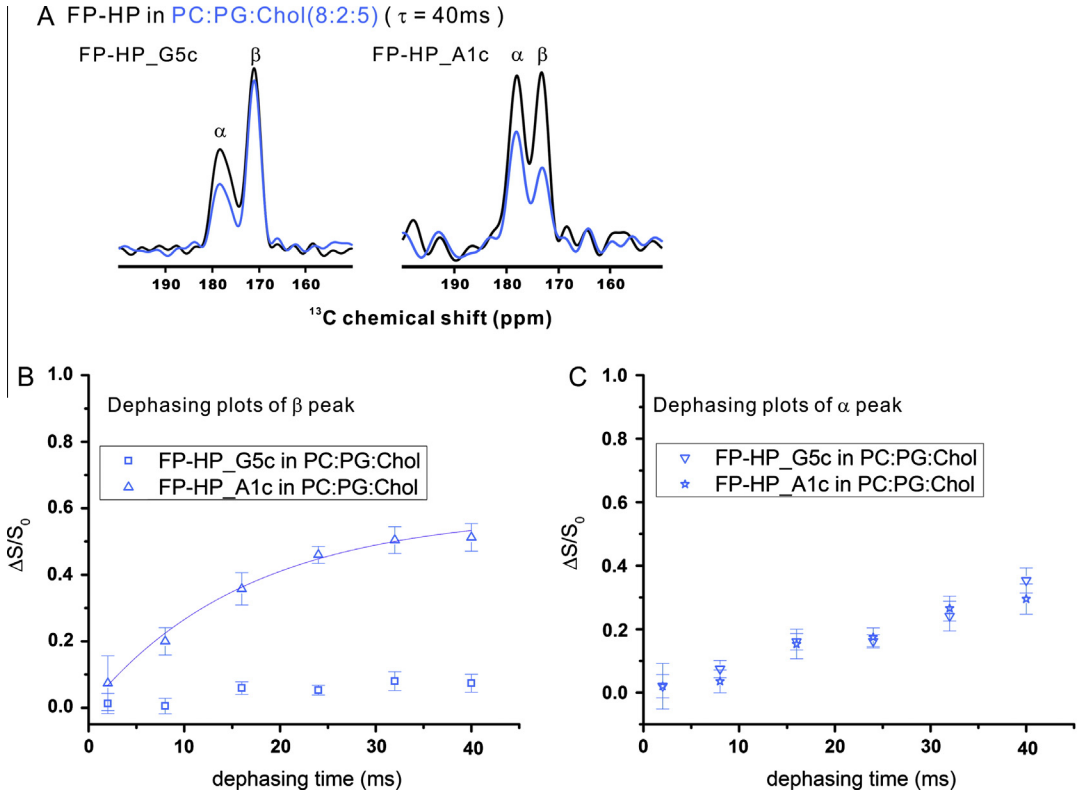

Fig. 8. ^{13}CO–^{31}P REDOR data from samples that contain either FP-HP_G5$_C$ or FP-HP_A1$_C$ in PC:PG:Chol (8:2:5) membrane. Panel A displays the S_0 (black) and S_1 (blue) REDOR spectra for τ = 40 ms. Plots of $(\Delta S/S_0)^{exp}$ vs τ are displayed for the (B) *lab* G5 and A1 β peaks and (C) *na* α peaks. The solid line in panel B is the fit of the A1 β data to $A \times (1 - e^{-\gamma\tau})$ with best-fit γ = 60(8) Hz and A = 0.58(3). (For interpretation of the references to color in this figure legend, the reader is referred to the web version of this article.)

$A_{d10} \approx 2A_{d8}$. These data support multiple membrane locations for β IFP as for β HFP with major and minor populations having respective deeper and shallower locations in the hydrocarbon core (Fig. 7).

For the samples described in the present publication, it is unlikely that cooling affects the membrane location of the protein because the membrane remains in the same phase, either gel-phase for membrane without Chol or liquid-ordered phase for membrane with 0.33 mol fraction Chol [50].

3. Discussion

3.1. Overview of ^{13}CO–^{2}H REDOR

The ^{13}CO–^{2}H REDOR experiment is robust with alternating ^{13}C and ^{2}H hard π pulses (Fig. 2). For ^{2}H rf fields of ~100 kHz, the $(\Delta S/S_0)^{exp}$ are not impacted by the ^{2}H quadrupolar anisotropy [20]. The effect of ^{2}H T_1 relaxation is modeled by each ^{2}H spending equal fractions of the dephasing time in the three m states. This results in exponential rather than sigmoidal buildup with buildup extent ≈ 1 and rate $\gamma \approx 2d/3$ (Fig. 3 and Table 2). The d reflects the average magnitude of the ^{2}H dipolar field at the *lab* ^{13}CO nuclei. For a single *lab* ^{13}CO nucleus, the field will have contributions from multiple ^{2}H nuclei with dependence on the r's and relative orientations of the internuclear vectors. In addition, the non-crystalline membrane environment means there will be some distribution of ^{2}H geometries and fields among ^{13}CO nuclei. Despite this complexity, the r's calculated using the single spin-pair approximation are in the 4–5 Å range which is consistent with van der Waals contact between the peptide sidechains and the lipid acyl $-CH_2$ and $-CH_3$ groups. The samples appeared to have thermodynamic equilibrium membrane locations (Fig. 4).

3.2. Major deep and minor shallow insertion of β sheet HFP

The different ^{13}CO–^{2}H and ^{13}CO–^{31}P REDOR buildups describe proximity of the *lab* residue to different membrane locations. For the present study, the extensive *lab* G5 data are self-consistent, e.g. deep insertion rather than interfacial location of G5 is evidenced by large ^{13}CO–^{2}H buildup with PC_d10 and Chol_d7, much smaller ^{13}CO–^{2}H buildup with PC_d4 and Chol_d6, and no ^{13}CO–^{31}P buildup (Figs. 1, 5A, 6A, and 8A). A previous ^{13}CO–^{2}H REDOR study using PC-d54 that contains perdeuterated acyl chains showed a rapid buildup to ~1. This supports insertion of all HFP molecules into the membrane hydrocarbon core.

We use $(\Delta S/S_0)^{exp}$ at τ = 48 ms and the best-fit A parameter as semi-quantitative estimates of the fractions of peptide molecules for which there is *lab* ^{13}C–^{2}H proximity. This is evidenced by $[(\Delta S/S_0)_{d8} + (\Delta S/S_0)_{d10}] \approx 1$ and $A_{d8} + A_{d10} \approx 1.3$ for the HFP samples (Fig. 5 and Table 2). For the HFP_G5$_C$ and HFP_L12$_C$ samples in PC:PG (4:1) membrane, there is *lab* ^{13}CO–^{2}H van der Waals contact with either PC_d8 or PC_d10 ($r \approx$ 4–5 Å) and the $[(\Delta S/S_0)_{d8}:(\Delta S/S_0)_{d10}] \approx$ 3:7 and $A_{d8}:A_{d10} \approx$ ~1:2 are interpreted to support a major HFP population that is deeply inserted and contacts PC_d10 ^{2}H's and a minor population that is more shallowly inserted and contacts PC_d8 ^{2}H's (Fig. 7). The REDOR data for β IFP are similar to those of β HFP and support two locations for β IFP (Fig. 9).

The multiple membrane locations of β sheet HFP may be due to or at least correlated with the distribution of HFP populations with different intermolecular antiparallel registries and hydrophobicities. Deeply-inserted HFP may induce local membrane perturbation that reduces the fusion activation energy to the highly perturbed fusion transition state. It is not clear whether or how the existence of major deeply-inserted and minor shallowly-inserted populations are advantageous to HIV. At least for

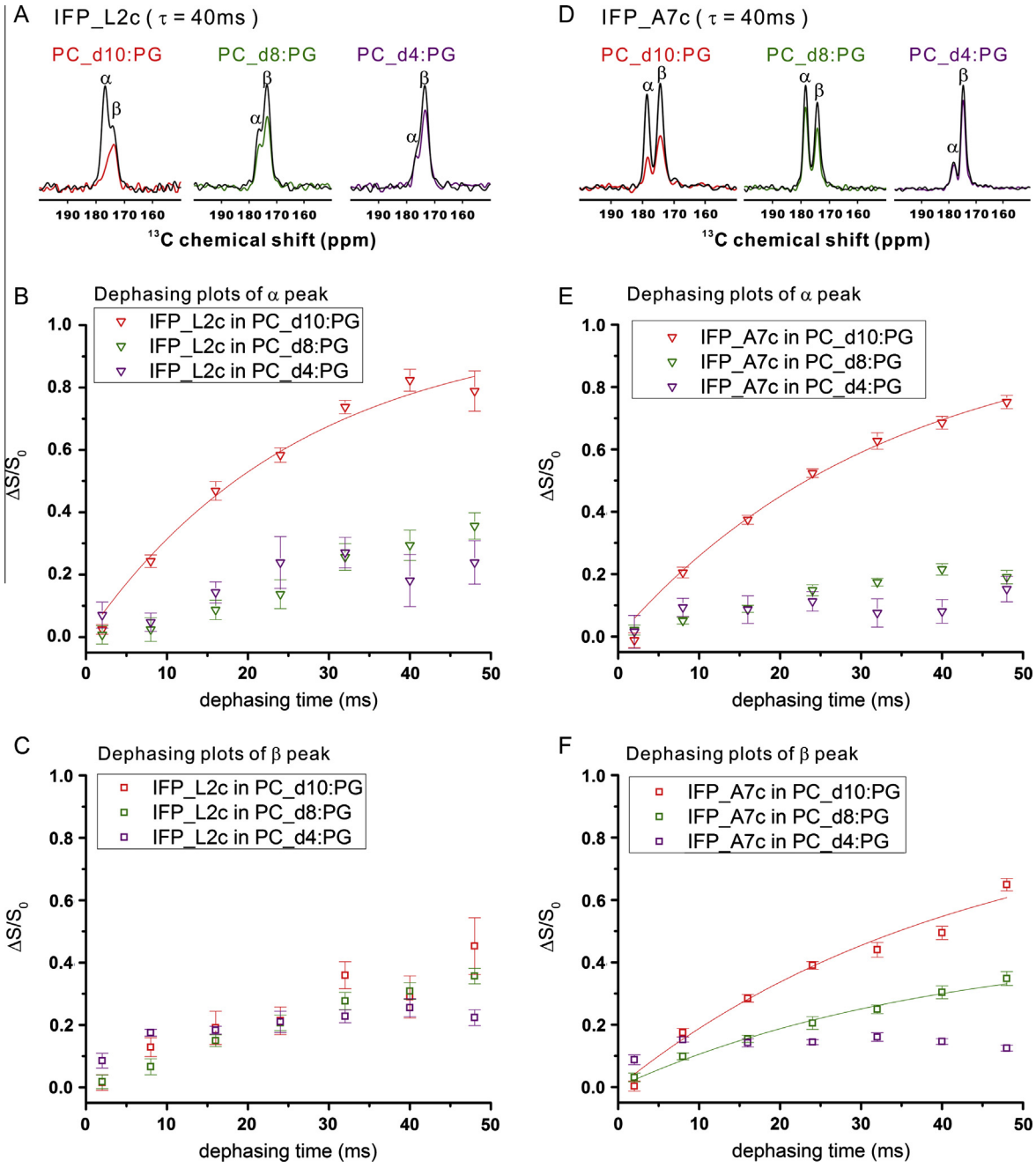

Fig. 9. $^{13}CO–^{2}H$ REDOR data from samples that contain either (A–C) IFP_L2$_C$ or (D–F) IFP_A7$_C$ in PC:PG (4:1) membrane. Samples were prepared with PC_d4, PC_d8, and PC_d10, and the corresponding data are displayed with colors that match those in Fig. 1. Panels A and D displays the S_0 (black) and S_1 (colored) REDOR spectra for $\tau = 40$ ms. Plots of $(\Delta S/S_0)^{exp}$ vs τ are displayed for the *lab* (B) L2 α, (C) L2 β, (E) A7 α, and (F) A7 β peaks. The solid lines are best-fits to $A \times (1 - e^{-\gamma\tau})$ and are done for substantial $(\Delta S/S_0)^{exp}$ buildups. (For interpretation of the references to color in this figure legend, the reader is referred to the web version of this article.)

membrane without Chol, the G5 ^{13}CO's of both HFP and the functionally-impaired HFP_V2E show similar buildups that support similar G5 membrane locations for both peptides (Fig. 5B, D). A more complete location model for HFP_V2E will require data with different *lab* sites. Data should also be obtained for membrane with Chol to correlate with the significant Chol fraction of host cell and HIV membranes. Earlier $^{13}CO–^{31}P$ REDOR for samples with Chol showed that relative to HFP, there is greater population of HFP_V2E in contact with membrane headgroup ^{31}P nuclei and presumably a smaller fraction in the membrane hydrocarbon core [25]. This difference supported a positive correlation between membrane insertion depth and fusogenicity.

3.3. Deep insertion of α helical IFP

IFP with *N*-helix/tight-turn/*C*-helix hairpin structure appears to have a single membrane location as evidenced by rapid IFP_L2$_C$ and IFP_A7$_C$ buildups in membrane with PC_d10 and correlate best-fit $A \approx 1$ (Fig. 9 and Table 2). Much smaller buildups were observed in membrane with PC_d8 and PC_d4. A single deep location is also supported by comparable buildups for IFP_L2$_C$ in membrane with PC_d10 or with perdeuterated PC_d54 [25]. The shared feature of deep insertion of the α IFP and β HFP fusion peptide structures may be relevant for fusion catalysis because of local perturbation of the membrane bilayer with consequent reduced activation energy to the highly perturbed fusion transition state. Deep

insertion of both the L2 and A7 residues is probably inconsistent with interfacial location of α IFP that was proposed to exist in detergent-rich media and also inconsistent with tilted membrane insertion based on EPR data [9,10,24,27]. A more complete model of the IFP membrane location will require additional ^{13}CO–^{2}H data with different *lab* sites including some in the *C*-helix region.

3.4. Comparison with other approaches

Relative to the more common relaxation-based methods, REDOR provides a clearer picture of different membrane locations of a residue as well as their relative populations (Fig. 7). Unlike fluorescence or EPR, ^{13}C–^{31}P or ^{13}C–^{2}H REDOR does not require chemical modification of the protein or membrane. Membrane location has also been probed with protein ^{13}C–membrane ^{19}F REDOR but this approach also requires chemically modified lipids prepared by custom synthesis of carboxylic acids with ^{1}H → ^{19}F substitution followed by lipid synthesis [5,25]. In addition, fluorinated lipid:total lipid is typically ⩽0.1 to prevent formation of non-lamellar phases and this low fraction results in a distribution of protein ^{13}C–lipid ^{19}F distances that is not straightforwardly deconvolved from the intrinsic distribution of membrane locations [51]. Finally, in our experience, it is difficult to tune well a probe to both ^{19}F and ^{1}H frequencies.

3.5. Future development and application of the REDOR approach

The samples of future studies could contain more complex mixtures of lipids and Chol including cell membrane extracts. The best-fit *r* and *A* values should be useful constraints in molecular dynamics (MD) simulations of the protein in explicit membrane and could also be used to assess the accuracy of simulations done without these constraints. The interpretation of the γ and *A* values is semi-quantitative because of the complexity of the spin systems and the locally non-crystalline nature of the membrane environment. Interpretation may be aided by comparison with MD simulations. Most data to-date were collected with a sample temperature of ∼−30 °C to reduce motional averaging of dipolar couplings so that couplings could be more directly related to distances. Buildups obtained at ∼0 °C are reduced presumably because of this averaging (Fig. 4). In the absence of Chol, there is gel-phase membrane at these lower temperatures whereas with Chol, there is a glassy liquid-ordered phase membrane [50]. There will be greater motional averaging near physiologic temperature so that probably only relative proximities and fractional populations can be determined via comparison of buildups in membranes with different ^{2}H labeling patterns.

The REDOR approach is applicable to larger proteins assuming that the ^{13}CO signal can be unambiguously assigned (Fig. 8). For FP-HP, this was aided by ligation of a selectively-labeled HFP to a larger expressed HP and also aided by the distinctive 171 ppm shift of *lab* Gly ^{13}CO's in β sheet structure. For α helical structure, *lab* Ala is a good choice because of the distinctive 179 ppm shift (Fig. 9).

One disadvantage of the REDOR approach is acquisition times of several days per sample. This is a consequence of ^{13}C detection, obtaining spectra at several dephasing times, and the T_2 signal loss associated with the needed 40–50 ms dephasing times for detection of ∼30 Hz couplings. The latter requirement probably precludes use of uniform ^{13}C-labeling for which T_2 would be further decreased because of the large ^{13}C–^{13}C couplings. Experimental sensitivity could be improved with use of lower temperatures or with low-temperature dynamic nuclear polarization prior to REDOR [52,53]. Low temperature also allows for the most quantitative interpretation of the REDOR buildups.

Obtaining unambiguous membrane location information by REDOR is time-intensive because of the previously discussed acquisition time per sample as well as the need for data from samples with different lipid and Chol ^{2}H labeling patterns and perhaps different protein ^{13}C labeling. The approach may find greatest use with systems like fusion proteins for which detailed residue-specific membrane location may be fundamental information needed to understand protein function.

One caveat of the typical interpretation of REDOR buildups is their correlation to locations of ^{31}P or ^{2}H nuclei in the membrane without protein (Fig. 1). The locations of the lipid or Chol that contact the protein may be different than the unperturbed locations [54,55]. In our view, this is also a caveat of most other approaches that probe membrane location. Experimental data may be better correlated to membrane location with information from MD simulations of the protein in explicit membrane and by new experimental approaches to probe the geometries of membrane molecules close to the protein.

In the future, it may be worth pursuing ^{13}C–^{2}H REDOR measurements of membrane location using ^{13}C-labeled lipid or Chol and protein with sidechains with ^{2}H labeling. Complementary information may also be obtained from measurements of ^{13}C–^{13}C couplings between ^{13}C-labeled protein and ^{13}C-labeled lipid or Chol. In our experience, reasonable analysis of ^{13}C–^{13}C couplings is only possible for experiments run under constant-time conditions with consequent longer signal-averaging times [42].

Acknowledgment

The research was supported by the National Institutes of Health grants R01 AI047153 and F32 AI080136. We thank the Michigan State University NMR and Mass Spectrometry facilities for their assistance with this research.

References

[1] Y. Su, R. Mani, M. Hong, Asymmetric insertion of membrane proteins in lipid bilayers by solid-state NMR paramagnetic relaxation enhancement: a cell-penetrating peptide example, J. Am. Chem. Soc. 130 (2008) 8856–8864.
[2] M. Michalek, C. Aisenbrey, B. Bechinger, Investigation of membrane penetration depth and interactions of the amino-terminal domain of huntingtin: refined analysis by tryptophan fluorescence measurement, Eur. Biophys. J. 43 (2014) 347–360.
[3] P.H. Lin, X. Chen, H. Moktan, E.L. Arrese, L. Duan, L.Y. Wang, J.L. Soulages, D.H.H. Zhou, Membrane attachment and structure models of lipid storage droplet protein 1, Biochim. Biophys. Acta 1838 (2014) 874–881.
[4] T. Gullion, J. Schaefer, Rotational-echo double-resonance NMR, J. Magn. Reson. 81 (1989) 196–200.
[5] O. Toke, W.L. Maloy, S.J. Kim, J. Blazyk, J. Schaefer, Secondary structure and lipid contact of a peptide antibiotic in phospholipid bilayers by REDOR, Biophys. J. 87 (2004) 662–674.
[6] L. Xie, U. Ghosh, S.D. Schmick, D.P. Weliky, Residue-specific membrane location of peptides and proteins using specifically and extensively deuterated lipids and ^{13}C–^{2}H rotational-echo double-resonance solid-state NMR, J. Biomol. NMR 55 (2013) 11–17.
[7] A. Agirre, C. Flach, F.M. Goni, R. Mendelsohn, J.M. Valpuesta, F.J. Wu, J.L. Nieva, Interactions of the HIV-1 fusion peptide with large unilamellar vesicles and monolayers. A cryo-TEM and spectroscopic study, Biochim. Biophys. Acta 1467 (2000) 153–164.
[8] M.E. Haque, V. Koppaka, P.H. Axelsen, B.R. Lentz, Properties and structures of the influenza and HIV fusion peptides on lipid membranes: implications for a role in fusion, Biophys. J. 89 (2005) 3183–3194.
[9] J.C. Macosko, C.H. Kim, Y.K. Shin, The membrane topology of the fusion peptide region of influenza hemagglutinin determined by spin-labeling EPR, J. Mol. Biol. 267 (1997) 1139–1148.
[10] X. Han, J.H. Bushweller, D.S. Cafiso, L.K. Tamm, Membrane structure and fusion-triggering conformational change of the fusion domain from influenza hemagglutinin, Nat. Struct. Biol. 8 (2001) 715–720.
[11] S. Maltsev, S.M. Hudson, I.D. Sahu, L.S. Liu, G.A. Lorigan, Solid-state NMR ^{31}P paramagnetic relaxation enhancement membrane protein immersion depth measurements, J. Phys. Chem. B 118 (2014) 4370–4377.
[12] K.K. Kumashiro, K. Schmidt-Rohr, O.J. Murphy, K.L. Ouellette, W.A. Cramer, L.K. Thompson, A novel tool for probing membrane protein structure: solid-state NMR with proton spin diffusion and X-nucleus detection, J. Am. Chem. Soc. 120 (1998) 5043–5051.
[13] G.J. Gallagher, M. Hong, L.K. Thompson, Solid-state NMR spin diffusion for measurement of membrane-bound peptide structure: gramicidin A, Biochemistry 43 (2004) 7899–7906.

[14] T. Wang, H. Yao, M. Hong, Determining the depth of insertion of dynamically invisible membrane peptides by gel-phase H-1 spin diffusion heteronuclear correlation NMR, J. Biomol. NMR 56 (2013) 139–148.
[15] D. Huster, X.L. Yao, M. Hong, Membrane protein topology probed by H-1 spin diffusion from lipids using solid-state NMR spectroscopy, J. Am. Chem. Soc. 124 (2002) 874–883.
[16] A. Schmidt, R.A. McKay, J. Schaefer, Internuclear distance measurement between Deuterium (I = 1) and a spin-1/2 nucleus in rotating solids, J. Magn. Reson. 96 (1992) 644–650.
[17] I. Sack, Y.S. Balazs, S. Rahimipour, S. Vega, Solid-state NMR determination of peptide torsion angles: applications of ^{2}H-dephased REDOR, J. Am. Chem. Soc. 122 (2000) 12263–12269.
[18] T. Gullion, R. Kishore, T. Asakura, Determining dihedral angles and local structure in silk peptide by ^{13}C–^{2}H REDOR, J. Am. Chem. Soc. 125 (2003) 7510–7511.
[19] J.D. Gehman, F. Separovic, K. Lu, A.K. Mehta, Boltzmann statistics rotational-echo double-resonance analysis, J. Phys. Chem. B 111 (2007) 7802–7811.
[20] L. Xie, L. Jia, S. Liang, D.P. Weliky, Multiple locations of peptides in the hydrocarbon core of gel-phase membranes revealed by peptide ^{13}C to lipid ^{2}H rotational-echo double-resonance solid-state nuclear magnetic resonance, Biochemistry 54 (2015) 677–684.
[21] J.M. White, S.E. Delos, M. Brecher, K. Schornberg, Structures and mechanisms of viral membrane fusion proteins: multiple variations on a common theme, Crit. Rev. Biochem. Mol. Biol. 43 (2008) 189–219.
[22] B. Apellaniz, N. Huarte, E. Largo, J.L. Nieva, The three lives of viral fusion peptides, Chem. Phys. Lipids 181 (2014) 40–55.
[23] M.T. Eddy, T.Y. Yu, Membranes, peptides, and disease: unraveling the mechanisms of viral proteins with solid state nuclear magnetic resonance spectroscopy, Solid State Nucl. Magn. Reson. 61–62 (2014) 1–7.
[24] J. Peuvot, A. Schanck, L. Lins, R. Brasseur, Are the fusion processes involved in birth, life and death of the cell depending on tilted insertion of peptides into membranes?, J Theor. Biol. 198 (1999) 173–181.
[25] W. Qiang, Y. Sun, D.P. Weliky, A strong correlation between fusogenicity and membrane insertion depth of the HIV fusion peptide, Proc. Natl. Acad. Sci. U. S. A. 106 (2009) 15314–15319.
[26] H.W. Yao, M. Hong, Conformation and lipid interaction of the fusion peptide of the paramyxovirus PIV5 in anionic and negative-curvature membranes from solid-state NMR, J. Am. Chem. Soc. 136 (2014) 2611–2624.
[27] J.L. Lorieau, J.M. Louis, A. Bax, The complete influenza hemagglutinin fusion domain adopts a tight helical hairpin arrangement at the lipid:water interface, Proc. Natl. Acad. Sci. U. S. A. 107 (2010) 11341–11346.
[28] E.O. Freed, E.L. Delwart, G.L. Buchschacher Jr., A.T. Panganiban, A mutation in the human immunodeficiency virus type 1 transmembrane glycoprotein gp41 dominantly interferes with fusion and infectivity, Proc. Natl. Acad. Sci. U. S. A. 89 (1992) 70–74.
[29] W. Qiang, M.L. Bodner, D.P. Weliky, Solid-state NMR spectroscopy of human immunodeficiency virus fusion peptides associated with host-cell-like membranes: 2D correlation spectra and distance measurements support a fully extended conformation and models for specific antiparallel strand registries, J. Am. Chem. Soc. 130 (2008) 5459–5471.
[30] S.D. Schmick, D.P. Weliky, Major antiparallel and minor parallel beta sheet populations detected in the membrane-associated Human Immunodeficiency Virus fusion peptide, Biochemistry 49 (2010) 10623–10635.
[31] J. Yang, P.D. Parkanzky, M.L. Bodner, C.G. Duskin, D.P. Weliky, Application of REDOR subtraction for filtered MAS observation of labeled backbone carbons of membrane-bound fusion peptides, J. Magn. Reson. 159 (2002) 101–110.
[32] Y. Sun, D.P. Weliky, ^{13}C–^{13}C Correlation spectroscopy of membrane-associated Influenza virus fusion peptide strongly supports a helix-turn-helix motif and two turn conformations, J. Am. Chem. Soc. 131 (2009) 13228–13229.
[33] U. Ghosh, L. Xie, D.P. Weliky, Detection of closed influenza virus hemagglutinin fusion peptide structures in membranes by backbone ^{13}CO–^{15}N rotational-echo double-resonance solid-state NMR, J. Biomol. NMR 55 (2013) 139–146.
[34] K. Sackett, M.J. Nethercott, Y. Shai, D.P. Weliky, Hairpin folding of HIV gp41 abrogates lipid mixing function at physiologic pH and inhibits lipid mixing by exposed gp41 constructs, Biochemistry 48 (2009) 2714–2722.
[35] P.U. Ratnayake, K. Sackett, M.J. Nethercott, D.P. Weliky, PH-dependent vesicle fusion induced by the ectodomain of the human immunodeficiency virus membrane fusion protein gp41: two kinetically distinct processes and fully-membrane-associated gp41 with predominant β sheet fusion peptide conformation, Biochim. Biophys. Acta 1848 (2015) 289–298.
[36] K. Banerjee, D.P. Weliky, Folded monomers and hexamers of the ectodomain of the HIV gp41 membrane fusion protein: potential roles in fusion and synergy between the fusion peptide, hairpin, and membrane-proximal external region, Biochemistry 53 (2014) 7184–7198.
[37] K. Sackett, A. TerBush, D.P. Weliky, HIV gp41 six-helix bundle constructs induce rapid vesicle fusion at pH 3.5 and little fusion at pH 7.0: understanding pH dependence of protein aggregation, membrane binding, and electrostatics, and implications for HIV-host cell fusion, Eur. Biophys. J. 40 (2011) 489–502.
[38] W. Qiang, D.P. Weliky, HIV fusion peptide and its cross-linked oligomers: efficient syntheses, significance of the trimer in fusion activity, correlation of β strand conformation with membrane cholesterol, and proximity to lipid headgroups, Biochemistry 48 (2009) 289–301.
[39] A.E. Bennett, C.M. Rienstra, M. Auger, K.V. Lakshmi, R.G. Griffin, Heteronuclear decoupling in rotating solids, J. Chem. Phys. 103 (1995) 6951–6958.
[40] T. Gullion, D.B. Baker, M.S. Conradi, New, compensated Carr-Purcell sequences, J. Magn. Reson. 89 (1990) 479–484.
[41] C.R. Morcombe, K.W. Zilm, Chemical shift referencing in MAS solid state NMR, J. Magn. Reson. 162 (2003) 479–486.
[42] Z. Zheng, R. Yang, M.L. Bodner, D.P. Weliky, Conformational flexibility and strand arrangements of the membrane-associated HIV fusion peptide trimer probed by solid-state NMR spectroscopy, Biochemistry 45 (2006) 12960–12975.
[43] M. Bak, J.T. Rasmussen, N.C. Nielsen, SIMPSON: a general simulation program for solid-state NMR spectroscopy, J. Magn. Reson. 147 (2000) 296–330.
[44] A.T. Petkova, Y. Ishii, J.J. Balbach, O.N. Antzutkin, R.D. Leapman, F. Delaglio, R. Tycko, A structural model for Alzheimer's beta-amyloid fibrils based on experimental constraints from solid state NMR, Proc. Natl. Acad. Sci. U. S. A. 99 (2002) 16742–16747.
[45] B. Brugger, B. Glass, P. Haberkant, I. Leibrecht, F.T. Wieland, H.G. Krasslich, The HIV lipidome: a raft with an unusual composition, Proc. Natl. Acad. Sci. U. S. A. 103 (2006) 2641–2646.
[46] F.B. Pereira, F.M. Goni, A. Muga, J.L. Nieva, Permeabilization and fusion of uncharged lipid vesicles induced by the HIV-1 fusion peptide adopting an extended conformation: dose and sequence effects, Biophys. J. 73 (1997) 1977–1986.
[47] K.F. Morris, X.F. Gao, T.C. Wong, The interactions of the HIV gp41 fusion peptides with zwitterionic membrane mimics determined by NMR spectroscopy, Biochim. Biophys. Acta 1667 (2004) 67–81.
[48] K. Sackett, M.J. Nethercott, R.F. Epand, R.M. Epand, D.R. Kindra, Y. Shai, D.P. Weliky, Comparative analysis of membrane-associated fusion peptide secondary structure and lipid mixing function of HIV gp41 constructs that model the early pre-hairpin intermediate and final hairpin conformations, J. Mol. Biol. 397 (2010) 301–315.
[49] M.L. Bodner, C.M. Gabrys, J.O. Struppe, D.P. Weliky, ^{13}C–^{13}C and ^{15}N–^{13}C correlation spectroscopy of membrane-associated and uniformly labeled HIV and influenza fusion peptides: amino acid-type assignments and evidence for multiple conformations, J. Chem. Phys. 128 (2008) 052319.
[50] M. Bloom, E. Evans, O.G. Mouritsen, Physical properties of the fluid lipid-bilayer component of cell membranes: a perspective, Quart. Rev. Biophys. 24 (1991) 293–397.
[51] D.J. Hirsh, N. Lazaro, L.R. Wright, J.M. Boggs, T.J. McIntosh, J. Schaefer, J. Blazyk, A new monofluorinated phosphatidylcholine forms interdigitated bilayers, Biophys. J. 75 (1998) 1858–1868.
[52] K.R. Thurber, R. Tycko, Biomolecular solid state NMR with magic-angle spinning at 25 K, J. Magn. Reson. 195 (2008) 179–186.
[53] K.R. Thurber, A. Potapov, W.M. Yau, R. Tycko, Solid state nuclear magnetic resonance with magic-angle spinning and dynamic nuclear polarization below 25 K, J. Magn. Reson. 226 (2013) 100–106.
[54] P. Larsson, P.M. Kasson, Lipid tail protrusion in simulations predicts fusogenic activity of influenza fusion peptide mutants and conformational models, PLoS Comp. Biol. 9 (2013) e1002950.
[55] E. Strandberg, S. Morein, D.T.S. Rijkers, R.M.J. Liskamp, P.C.A. van der Wel, J.A. Killian, Lipid dependence of membrane anchoring properties and snorkeling behavior of aromatic and charged residues in transmembrane peptides, Biochemistry 41 (2002) 7190–7198.
[56] S. Tristram-Nagle, J.F. Nagle, Lipid bilayers: thermodynamics, structure, fluctuations, and interactions, Chem. Phys. Lipids 127 (2004) 3–14.